# Face- and Cell-Averaged Nodal-Gradient Approach to Cell-Centered Finite-Volume Method on Mixed Grids

Hiroaki Nishikawa[*]

*National Institute of Aerospace, Hampton, VA 23666, USA*

Jeffery A. White[†]

*NASA Langley Research Center, Hampton VA 23681*

In this paper, the averaged nodal-gradient approach previously developed for triangular grids is extended to mixed triangular-quadrilateral grids. It is shown that the face-averaged approach leads to deteriorated iterative convergence on quadrilateral grids. To develop a convergent solver, we consider cell-averaging instead of face-averaging for quadrilateral cells. We show that the cell-averaged approach leads to a convergent solver and can be efficiently combined with the face-averaged approach on mixed grids. The method is demonstrated for various inviscid and viscous problems from low to high Mach numbers on two-dimensional mixed grids.

## 1. Introduction

This paper is a sequel to the AIAA Aviation 2019 paper "Face-Averaged Nodal-Gradient Approach to Cell-Centered Finite-Volume Method on Triangular Grids" [1], in which we proposed an efficient cell-centered finite-volume method based on the face-averaged nodal-gradients and the use of a common gradient in linear reconstruction at a face. The approach has several advantages over conventional cell-centered finite-volume methods on triangular grids, including less storage for least-squares gradient coefficients and more economical gradient computations, elimination of interpartition communication for gradients, and significantly more compact residual stencils. However, it has been found that the method has a serious drawback on quadrilateral grids. The objective of this paper is to investigate the issue and propose a suitable modification.

The face-averaged nodal-gradient (F-ANG) method is an efficient extension of the method of Zhang [2, 3, 4], who suggested to compute the cell-gradients by averaging the gradients computed at nodes with solutions stored at surrounding cells. In this way, the cost of gradient computations is dramatically reduced on triangular and tetrahedral grids, where the number of nodes is much smaller than the number of cells by a factor of approximately two in triangular grids and six in tetrahedral grids. Whereas Zhang computes the cell-gradient, for use in linear solution reconstructions, by averaging the nodal gradients over each cell, we proposed in Ref. [1] to average the nodal gradients over each face and use the same face gradient for linear reconstructions from both sides of the face. This reconstruction has been shown to work remarkably well on triangular grids, reducing the residual stencil and eliminating the need for interpartition communication of the gradient. However, when applied to a quadrilateral grid, the reconstruction stencil is too small in each coordinate direction and an implicit solver has been found not to converge well. In this paper, this problem is analyzed for a model equation and confirmed theoretically by a Fourier analysis. As a remedy, we propose a mixed strategy, where the face-averaged approach is used for inviscid terms on triangles and the cell-averaged approach for quadrilaterals, i.e., reverting to Zhang's approach, and demonstrate it for inviscid and viscous flow problems on quadrilateral and mixed grids.

---

[*]Associate Research Fellow (hiro@nianet.org), 100 Exploration Way, Hampton, VA 23666 USA, Associate Fellow AIAA
[†]Senior Research Scientist (jeffery.a.white@nasa.gov), Computational AeroSciences Branch, Mail Stop 128, Associate Fellow AIAA

American Institute of Aeronautics and Astronautics

## 2. Governing Equations

Consider the compressible Navier-Stokes (NS) equations in two dimensions:

$$\frac{\partial \mathbf{u}}{\partial t} + \frac{\partial \mathbf{f}_x}{\partial x} + \frac{\partial \mathbf{f}_y}{\partial y} = 0, \tag{2.1}$$

where

$$\mathbf{u} = \begin{bmatrix} \rho \\ \rho u \\ \rho v \\ \rho E \end{bmatrix}, \quad \mathbf{f}_x = \mathbf{f}_x^{inv} + \mathbf{f}_x^{vis} = \begin{bmatrix} \rho u \\ \rho u^2 + p \\ \rho uv \\ \rho uH \end{bmatrix} + \begin{bmatrix} 0 \\ -\tau_{xx} \\ -\tau_{xy} \\ -\tau_{xx}u - \tau_{xy}v + q_x \end{bmatrix}, \tag{2.2}$$

$$\mathbf{f}_y = \mathbf{f}_y^{inv} + \mathbf{f}_y^{vis} = \begin{bmatrix} \rho v \\ \rho uv \\ \rho v^2 + p \\ \rho vH \end{bmatrix} + \begin{bmatrix} 0 \\ -\tau_{yx} \\ -\tau_{yy} \\ -\tau_{yx}u - \tau_{yy}v + q_y \end{bmatrix}, \tag{2.3}$$

$\rho$ is the density, $(u, v)$ is the velocity vector, $p$ is the pressure, $E$ is the specific total energy, and $H = E + p/\rho$ is the specific total enthalpy. The viscous stresses $(\tau_{xx}, \tau_{xy}, \tau_{yy})$, and the heat fluxes $q_x$ and $q_y$ are given by

$$\tau_{xx} = \frac{2}{3}\mu \left( 2\frac{\partial u}{\partial x} - \frac{\partial v}{\partial y} \right), \quad \tau_{xy} = \tau_{yx} = \mu \left( \frac{\partial u}{\partial y} + \frac{\partial v}{\partial x} \right), \quad \tau_{yy} = \frac{2}{3}\mu \left( 2\frac{\partial v}{\partial y} - \frac{\partial u}{\partial x} \right), \tag{2.4}$$

$$q_x = -\frac{\mu}{Pr(\gamma - 1)}\frac{\partial T}{\partial x}, \quad q_y = -\frac{\mu}{Pr(\gamma - 1)}\frac{\partial T}{\partial y}. \tag{2.5}$$

where $T$ is the temperature, $\gamma$ is the ratio of specific heats, $Pr$ is the Prandtl number, and $\mu$ is the viscosity defined by Sutherland's law. All the quantities are assumed to have been nondimensionalized by their free-stream values except that the velocity and the pressure are scaled by the free-stream speed of sound and the dynamic pressure based on the free-stream speed of sound, respectively (see Ref. [5]). Thus, the viscosity is given by the following form of Sutherland's law:

$$\mu = \frac{M_\infty}{Re_\infty}\frac{1 + C/\tilde{T}_\infty}{T + C/\tilde{T}_\infty}T^{\frac{3}{2}}, \tag{2.6}$$

where $\tilde{T}_\infty$ is the dimensional free stream temperature in Kelvin (K), and $C = 110.5$ K is the Sutherland constant. The ratio of the free stream Mach number $M_\infty$ to the free stream Reynolds number $Re_\infty$ arises from the nondimensionalization. The system is closed by the nondimensionalized equation of state for ideal gases: $\gamma p = \rho T$.

## 3. Finite-Volume Discretization

A cell-centered finite-volume discretization is defined as an approximation to the NS system integrated over a computational cell $j$ (see Figure 1) with the midpoint rule:

$$\mathbf{Res}_j = \sum_{k \in \{k_j\}} \mathbf{\Phi}_{jk} A_{jk}, \tag{3.1}$$

where $\{k_j\}$ is a set of neighbors of the cell $j$, $A_{jk}$ is the length of the face across $j$ and $k$, and $\mathbf{\Phi}_{jk}$ is a numerical flux, which is a function of the left and right states and the gradients:

$$\mathbf{\Phi}_{jk} = \mathbf{\Phi}_{jk}(\mathbf{w}_L, \mathbf{w}_R, \nabla\mathbf{w}_L, \nabla\mathbf{w}_R), \tag{3.2}$$

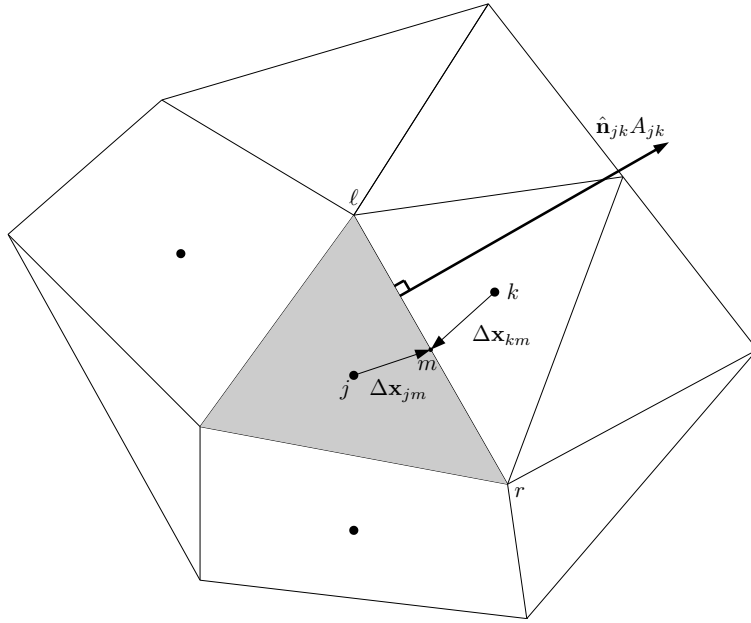American Institute of Aeronautics and Astronautics

Figure 1: Stencil for cell-centered finite-volume discretization.

$\mathbf{w} = (\rho, u, v, p)$. In this work, the Roe [6] and HLL [7] fluxes are used for the inviscid terms, and the alpha-damping flux [8, 9, 10, 11] for the viscous terms. The solution values are stored at cells as point values at the centroid. Second-order accuracy is achieved by the linearly-exact flux quadrature (i.e., the midpoint rule) and the linearly reconstructed solutions at the face midpoint $m$:

$$\mathbf{w}_L = \mathbf{w}_j + \nabla \mathbf{w}_j \cdot \Delta \mathbf{x}_{jm}, \quad \mathbf{w}_R = \mathbf{w}_k + \nabla \mathbf{w}_k \cdot \Delta \mathbf{x}_{km}, \tag{3.3}$$

$$\nabla \mathbf{w}_L = \nabla \mathbf{w}_j, \quad \nabla \mathbf{w}_R = \nabla \mathbf{w}_k, \tag{3.4}$$

which requires the gradients at cells, $\nabla \mathbf{w}_j$ and $\nabla \mathbf{w}_k$. In the proposed approach, these gradients are computed from gradients at nodes, which are computed by a linear LSQ method using the cells surrounding each node, as described in detail in Ref. [1].

## 4. Face- and Cell-Averaged Nodal-Gradients

In the previous work [1], we have demonstrated that the reconstruction with a common face-averaged gradient offers several advantages over a conventional cell-gradient method:

$$\mathbf{w}_L = \mathbf{w}_j + \nabla \mathbf{w}_f \cdot \Delta \mathbf{x}_{jm}, \quad \mathbf{w}_R = \mathbf{w}_k + \nabla \mathbf{w}_f \cdot \Delta \mathbf{x}_{km}, \tag{4.1}$$

$$\nabla \mathbf{w}_L = \nabla \mathbf{w}_f, \quad \nabla \mathbf{w}_R = \nabla \mathbf{w}_f, \tag{4.2}$$

where $\nabla \mathbf{w}_f$ denotes a common face gradient given by

$$\nabla \mathbf{w}_f = \frac{1}{2} \left( \nabla \mathbf{w}_{jk}^{\ell} + \nabla \mathbf{w}_{jk}^{r} \right), \tag{4.3}$$

where the superscripts $\ell$ and $r$ denote the left and right nodes of the face $[j, k]$ (see Figure 1). For example, the storage for and cost of computing the gradients are reduced by a factor of two on triangular grids and around six in tetrahedral grids, the resulting residual stencil is greatly reduced. Moreover, it eliminates interpartition communication for the gradients. This method of reconstruction is the F-ANG method.

American Institute of Aeronautics and Astronautics

However, as we will show, this approach does not result in a satisfactory scheme for quadrilateral grids, causing serious convergence issues. To overcome the problem, we consider cell-averaging instead of face-averaging for quadrilateral cells:

$$\mathbf{w}_L = \mathbf{w}_j + \nabla \mathbf{w}_j \cdot \Delta \mathbf{x}_{jm}, \quad \mathbf{w}_R = \mathbf{w}_k + \nabla \mathbf{w}_k \cdot \Delta \mathbf{x}_{km}, \tag{4.4}$$

where

$$
\nabla \mathbf{w}_j =
\begin{cases}
\dfrac{1}{4} \sum_{i \in \{i_j\}} \nabla \mathbf{w}_i, & \text{if the cell } j \text{ is a quadrilateral,} \\[2ex]
\dfrac{1}{2} \left( \nabla \mathbf{w}_{jk}^\ell + \nabla \mathbf{w}_{jk}^r \right) & \text{if the cell } j \text{ is a triangle.}
\end{cases}
\tag{4.5}
$$

where $\{i_j\}$ denotes the set of four vertices of the quadrilateral $j$, and similarly for the other gradient, $\nabla \mathbf{w}_k$. The cell-averaging is the approach originally considered by Zhang [2,3,4]; it is employed here only for a linear reconstruction within a quadrilateral cell. For quadrilateral cells, the cell-averaging introduces an additional neighbor to the residual stencil in the direction normal to each face, which is included in a conventional finite-volume discretization but not in the F-ANG. These additional neighbors are considered as necessary for stable convergence and here they are introduced by the cell-averaging approach. The resulting method is referred to as the face-and-cell-averaged-nodal-gradient (FAC-ANG) method in the rest of the paper. See Ref. [12] for further details, concerning its extensions to three-dimensional unstructured grids.

Note that the cell-averaging method has a drawback that the averaged cell-gradients need to be communicated across partition boundaries in parallel computations, whereas it was not necessary in F-ANG. It is possible to skip the communication for tetrahedral cells, but it is simpler in terms of implementation to perform the communication in all cells. Also, the residual stencil becomes as large as the conventional method with the node-neighbor gradient stencil although it remains as small as F-ANG for the tetrahedral part of a grid. An improved approach in these aspects is currently under development and will be reported in a subsequent paper.

## 4.1. Limiter

A limiter function is needed to deal with shock waves and they are applied to the reconstruction as

$$\mathbf{w}_L = \mathbf{w}_j + \phi_j \nabla \mathbf{w}_j \cdot \Delta \mathbf{x}_{jm}, \quad \mathbf{w}_R = \mathbf{w}_k + \phi_k \nabla \mathbf{w}_k \cdot \Delta \mathbf{x}_{km}, \tag{4.6}$$

where $\phi_j$ and $\phi_k$ are the limiter functions defined in the cell $j$ and $k$, respectively. In this study, the limiter is defined in each cell by applying the Venkat limiter [13] based on the vertex enforcement as described in Ref. [14]. The minimum and maximum values are found from the node-neighbor stencil of the cell, which is the union of nodal LSQ gradient stencils over the cell. The limiter function is defined by the minimum, as typically done, of those computed for all face gradients in a cell, at all faces, and all primitive variables. See Ref. [1] for details.

# 5.   Nonlinear Solver

To solve the global nonlinear residual equations,

$$0 = \mathbf{Res}(\mathbf{U}), \tag{5.1}$$

we consider the implicit defect-correction solver as we have used in the previous work [1]

$$\mathbf{U}^{n+1} = \mathbf{U}^n + \Delta \mathbf{U}, \tag{5.2}$$

$$\left( \mathbf{D} + \frac{\partial \overline{\mathbf{Res}}}{\partial \mathbf{U}} \right) \Delta \mathbf{U} = -\mathbf{Res}(\mathbf{U}^n), \tag{5.3}$$

where $n$ is the iteration counter, $\mathbf{D}$ is the pseudotime diagonal matrix with the $j$-th diagonal block, which corresponds to the cell $j$, is defined by $\mathbf{D}_{jj} = V_j/\Delta \tau_j \, \mathbf{I}$, where $\mathbf{I}$ is the 4×4 identity matrix and $\Delta \tau_j$ is

a local pseudotime step, and the Jacobian $\partial \overline{\mathbf{Res}}/\partial \mathbf{U}$ is the exact differentiation of the low-order compact residual $\overline{\mathbf{Res}}$ with zero gradients (i.e., first-order accurate for the inviscid terms and zeroth order for the viscous terms). Note that the number of off-diagonal blocks in the Jacobian is the same as the number of face neighbors. The pseudotime step is defined at a cell $j$ by

$$\Delta \tau_j = \text{CFL} \frac{2V_j}{\displaystyle\sum_{k \in \{k_j\}} [\, |u_n| + a + a_h \,] A_{jk}}, \quad a_h = \frac{2\alpha\gamma\mu}{\rho Pr |(\Delta\mathbf{x}_{jm} - \Delta\mathbf{x}_{km}) \cdot \hat{\mathbf{n}}_{jk}|}, \tag{5.4}$$

where $V_j$ is the volume of the cell $j$, $u_n$ is the flow speed in the direction normal to the face, $a$ is the speed of sound at the face, and $a_h$ is a characteristic speed associated with the viscous heating wave (see Ref. [9]) defined with the damping parameter $\alpha = 4/3$, the ratio of specific heats $\gamma = 1.4$, the Prandtl number $P_r = 0.72$. The linear system is relaxed by the multicolor block Gauss-Seidel relaxation scheme, which is written for a cell $j$ as

$$\Delta\mathbf{u}_j^{m+1} = \Delta\mathbf{u}_j^m + \omega\mathbf{r}_j, \quad \mathbf{r}_j = \left(\frac{\partial\overline{\mathbf{Res}}_j}{\partial\mathbf{u}_j}\right)^{-1}\left[\sum_{k \in \{k_j\}} \frac{\partial\overline{\mathbf{Res}}_j}{\partial\mathbf{u}_k} - \mathbf{Res}_j(\mathbf{U}^n)\right], \tag{5.5}$$

where $\mathbf{Res}_j$ is the residual vector in the cell $j$, $m$ is the relaxation counter, $\omega$ is a relaxation factor, and $\frac{\partial\overline{\mathbf{Res}}_j}{\partial\mathbf{u}_j}$ and $\frac{\partial\overline{\mathbf{Res}}_j}{\partial\mathbf{u}_k}$ are the 4×4 diagonal and off-diagonal matrices, respectively. It is noted that the implicit solver is based on the Jacobian with zero gradients and therefore there is no difference for the conventional gradient approach and the proposed approach. The only difference is in the residual on the right hand side.

## 6.   Fourier Analysis

As mentioned earlier and will be numerically shown later, the F-ANG method does not lead to a convergent solver on quadrilateral grids. It may be due to lack of solution jump in the dissipation term in each coordinate direction, which resembles one-dimensional schemes, where the F-ANG method gives exactly $\mathbf{w}_R - \mathbf{w}_L = 0$. In this section, we demonstrate by a Fourier analysis that the problem is observed even for a linear advection on a Cartesian grid, with the spacing $h$, but can be successfully resolved by the cell-averaging approach. Consider a Fourier mode:

$$u^\beta = u_0^\beta \exp\left(i\left\{\beta_x\frac{x}{h} + \beta_y\frac{y}{h}\right\}\right), \tag{6.1}$$

where $u_0^\beta$ is the amplitude, $\beta_x$ and $\beta_y$ are frequencies (phase changes per grid spacing) in the $x$ and $y$ directions, respectively. Substituting the Fourier mode into Equation (5.2) applied to solve a linear advection equation, $a\partial_x u + b\partial_y u = 0$, where $a$ and $b$ are constants, we obtain for CFL $\to \infty$

$$(u_0)^{n+1} = \rho(\beta_x, \beta_y)\,(u_0)^n, \quad \rho(\beta_x, \beta_y) = 1 - \frac{\lambda_R}{\lambda_J}, \tag{6.2}$$

where $\lambda_R$ is the residual operator and $\lambda_J$ is the Jacobian operator. The convergence rate of the implicit solver is determined by the maximum of $|\rho|$ taken over all frequencies:

$$\rho_{max} = \max_{\beta_x, \beta_y \in (0,\pi)} |\rho(\beta_x, \beta_y)|. \tag{6.3}$$

The solver is convergent if $\rho_{max} < 1$ and otherwise not convergent.

For simplicity but without loss of generality, we assume $a > 0$ and $b > 0$. For the F-ANG method, we obtain

$$\rho(\beta_x, \beta_y) = \frac{[(a+b)\cos(\beta_y) + (a-b)]\cos(\beta_x) - (a-b)\cos(]beta_y) - (a+b)}{2[a\exp(-i\beta_x) + b\exp(-i\beta_y) - (a+b)]}. \tag{6.4}$$

It suffices to consider the case with $(a,b) = (1,1)$ at $(\beta_x, \beta_y) = (0,\pi)$ and $(\beta_x, \beta_y) = (\pi, 0)$, for which we find $|\rho(\beta_x, \beta_y)| = 1$, i.e., the F-ANG method is not convergent on a regular quadrilateral grid. In contrast, for the conventional method with the face-neighbor gradient stencil (i.e., four neighbors), we then obtain

$$\rho(\beta_x, \beta_y) = \frac{a\exp(-2i\beta_x) + b\exp(-2i\beta_y) + 2i[a\sin(\beta_x) + b\sin(\beta_y)] - (a+b)}{4[a\exp(-i\beta_x) + b\exp(-i\beta_y) - (a+b)]}, \tag{6.5}$$

American Institute of Aeronautics and Astronautics

whose magnitude achieves the maximum magnitude of 0.5 for $(a, b) = (1, 1)$ at $(\beta_x, \beta_y) = (\pi/2, \pi/2)$. This scheme is known to be stable. See Ref[15] for details. Finally, for the FAC-ANG method (which is practically C-ANG for the pure quadrilateral grid), we obtain

$$\rho(\beta_x, \beta_y) = \frac{1}{16[a \exp(-i\beta_x) + b \exp(-i\beta_y) - (a+b)]} [a \exp(-i(2\beta_x - \beta_y)) + a \exp(-i(2\beta_x + \beta_y))$$

$$+ b \exp(-i(\beta_x + 2\beta_y)) + b \exp(i(\beta_x - 2\beta_y)) + 2i(a - b) \sin(\beta_x - \beta_y)$$

$$- (2a + b) \exp(-i\beta_x) - (a + 2b) \exp(-i\beta_y) + 2a \exp(-2i\beta_x)$$

$$+ 2b \exp(-2i\beta_y) + (2a - b) \exp(i\beta_x) - (a - 2b) \exp(i\beta_y) + 2(i \sin(\beta_x + \beta_y) - 1)(a + b)], \quad (6.6)$$

whose magnitude again achieves the maximum magnitude of 0.5 for $(a, b) = (1, 1)$ at $(\beta_x, \beta_y) = (\pi/2, \pi/2)$. Therefore, the FAC-ANG method is as convergent as the conventional method for this particular advection vector. It is convergent for more general cases as we will later demonstrate numerically.

For diffusion, the Fourier analysis shows that the F-ANG method leads to convergence; the details will be reported elsewhere. However, as we will see later, the use of F-ANG for the viscous terms results in slower convergence for the Navier-Stokes equations.

# 7.   Numerical Results

In this section, the FAC-ANG method is demonstrated for various test cases and compared with a conventional method with the node-neighbor gradient stencil, which is referred to as the node-neighbor-cell-centered-gradient (NN-CCG). Here, the node-neighbor gradient stencil is used, rather than the face-neighbor stencil, because it is known that the solver can get unstable with the latter but stable with the former on triangles [16]. Unless otherwise stated, 50 Gauss-Seidel relaxation are performed per nonlinear iteration; the Jacobian gets frozen after three orders of residual reduction and then will be updated at every one order reduction thereafter; and the CFL number is initially set to be 10, linearly increased to 100 over the first 15 iterations, and then increased by a factor of 10 up to $10^6$ when the residual norm decreases. The under-relaxation parameter $\omega$ will be reduced to keep the density and pressure positive when negative density and/or pressure is detected in the solution update. Therefore, the only differences are the gradient calculation and the use of the face gradient in the solution reconstruction. The residual convergence will be shown in the maximum $L_1$ residual norm scaled by the initial norm over all equations. A steady state is taken to be reached when the maximum residual norm is reduced by six orders of magnitude. Solution contours will be plotted based on the nodal value computed by averaging linearly-interpolated solutions from within all cells sharing a node; thus second-order accuracy is retained. The under-relaxation parameter $\omega$ is set to be 1.0 for all cases except the hypersonic flow case, where we set $\omega = 0.25$.

## 7.1.   Euler Equations

### 7.1.1.   Subsonic flow over a circular cylinder at $M_\infty = 0.3$

We consider an inviscid compressible flow over a circular cylinder at $M_\infty = 0.3$. The domain is defined by the cylinder of unit diameter and the circular outer boundary of radius 100. The problem is solved on a quadrilateral grid shown in Figures 2(a) and 2(b): 3,200 quadrilaterals and 80 nodes over the cylinder. The limiter is not used. Boundary conditions are imposed weakly through the numerical flux via the right state: free stream condition at the left half of the outer boundary, a back-pressure condition (the free stream pressure is specified) at the right half of the outer boundary, and a slip condition at the cylinder. Figure 2(c) shows the convergence results. As can be seen, F-ANG eventually diverged whereas FAC-ANG and NN-CCG converged very rapidly. Solutions obtained with NN-CCG and FAC-ANG are very similar to each other as shown in Figures 2(d) and 2(e). As expected, the results confirm that the cell-averaged nodal-gradient approach resolves the issue of F-ANG on quadrilateral grids.

### 7.1.2.   Transonic flow over a Joukowsky airfoil at $M_\infty = 0.8$

To compare NN-CCG, F-ANG, and FAC-ANG with a limiter, we consider a transonic flow over a Joukowsky airfoil of a unit chord at $M_\infty = 0.8$ at the angle of attack 1.25 degrees. The outer bound-

ary is taken as a circle of radius 50. The domain is divided into quadrilaterals as shown in Figures 3(a) and 3(b): 2093 quadrilaterals, 2184 nodes with 92 nodes over the airfoil. Figure 3(c) shows the iterative convergence results. Somewhat surprisingly, all NN-CCG, F-ANG, FAC-ANG converged to the specified tolerance although F-ANG takes more iterations. It indicates that the F-ANG method can be made convergent with a limiter. Figure 3(d) compares the pressure distributions over the airfoil. As can be seen, there are no significant differences in the solutions. See also Figures 3(e)-3(g), where very similar pressure contours can be observed.

### 7.1.3.  Hypersonic flow over a cylinder at $M_\infty = 5.2$

To further investigate the effect of limiting, we consider a hypersonic flow over a cylinder at $M_\infty = 5.2$ on a quadrilateral grid as shown in Figures 4(a) and 4(b): 1024 quadrilaterals and 1089 nodes with 33 nodes over the cylinder surface. For this problem, the CFL number is ramped from 0.1 to 100 over 10,000 iterations. Also, the HLL flux is employed instead of Roe, and the exact derivative of the Rusanov flux [17] is used in the Jacobian. Furthermore, the solution update is limited to 25% of the full update at every iteration (i.e., $\omega = 0.25$).

Figure 4(c) shows the iterative convergence results. Again, all methods lead to convergence, where NN-CCG takes the least number of iterations. As in the previous case, the solver converged for the F-ANG method with a limiter. As shown in Figures 4(d)-4(f), all the methods result in very similar solutions.

## 7.2.  Navier-Stokes Equations

### 7.2.1.  Viscous flow over a circular cylinder at $M_\infty = 0.3$ and $Re_\infty = 20$

We consider a viscous flow over a circular cylinder at $M_\infty = 0.3$ and $Re_\infty = 20$ with a mixed grid (3,200 nodes, 3,840 triangles, 1200 quadrilaterals) as shown in Figures 5(a),. The no-slip viscous wall condition is applied at the cylinder weakly through the numerical flux with zero velocity and the free stream temperature given in the right state. The inflow and outflow conditions are the same as those in the inviscid case.

Iterative convergence results are shown in Figure 5(b). As expected, the solver significantly slows down for F-ANG while it converges rapidly for NN-CCG and FAC-ANG. We tested also a combination of FAC-ANG for the inviscid terms and F-ANG for the viscous terms, which is indicated as FAC-ANG (F-ANG-vis) in the plot. As shown, the solver slows down although not as slow as F-ANG.

### 7.2.2.  Viscous flow over a flat plate at $M_\infty = 0.15$ and $Re_\infty = 10^6$

Finally, we consider a high-Reynolds-number laminar flow over a flat plate at $M_\infty = 0.15$ and $Re_\infty = 10^6$. The grid is a mixed grid with 10,608 triangles and 3,120 quadrilaterals in the boundary-layer region, and 80 nodes placed over the flat plate located at $y = 0$ and $x \in [0, 2]$. See Figures 6(a) and 6(b). In this case, F-ANG exhibits an erratic convergence behavior while NN-CCG and FAC-ANG lead to convergence as can be seen Figure 6(c). Nevertheless, it managed to reduce the residual to the tolerance. The FAC-ANG (F-ANG-vis) method leads to convergence without a significant slow-down as before, but takes more iterations to converge. In terms of accuracy, F-ANG yields a better agreement with the Blasius solution for the $y$-component of the velocity as shown in Figure 6(e) sampled along the vertical grid line at $x = 0.9$. It is conjectured that the superior accuracy is due to the reduced dissipation on quadrilaterals as mentioned earlier. The vorticity was computed at nodes by averaging the cell-gradients over the cells surrounding a node in NN-CCG, and directly evaluated by the nodal gradients in F-ANG, FAC-ANG, and FAC-ANG (F-ANG-vis). The comparison for the vorticity shown in Figure 6(f) shows that the computation at nodes is more accurate.

# 8.  Concluding Remarks

We have shown that the F-ANG method does not lead to a practical solver for quadrilateral and mixed grids. A Fourier analysis shows that it does not lead to a convergent solver for a linear advection equation on a regular quadrilateral grid. Numerical results show that the solver diverges or significantly slows down for F-ANG on grids with quadrilateral cells. One possible remedy is to employ the cell-averaged nodal-gradient (C-ANG) method as originally proposed by Zhang. The convergence of the solver has been confirmed by the Fourier analysis for the model equation and demonstrated for inviscid and viscous flow problems

on quadrilateral and mixed grids. The FAC-ANG method has been successfully implemented in NASA's VULCAN code, and encouraging results are presented in a companion paper [12].

Although the issue with F-ANG on mixed grids has been successfully resolved by the FAC-ANG approach, it results in a larger residual stencil (equivalent to the conventional method with the vertex-neighbor gradient stencil) and interpartition communication will be required for cell-gradients in a parallel code (which is not required in F-ANG). In order to preserve these benefits as much as possible, a different approach is currently being developed, which aims also at achieving higher-order accuracy in case of regular quadrilateral grids, and will be reported in a subsequent paper.

# Acknowledgments

# References

[1]Nishikawa, H. and White, J. A., "Face-Averaged Nodal-Gradient Approach to Cell-Centered Finite-Volume Method on Triangular Grids," *24th AIAA Computational Fluid Dynamics Conference*, AIAA Paper 2019-3636, Dallas, TX, 2019.

[2]Zhang, F., Liu, J., Chen, B., and Zhong, W., "A Nodal-Weighted-Least-Squares Gradient Reconstruction for Cell-Centered Finite Volume Method," Unpublished, 2015.

[3]Zhang, F., "A Vertex-Weighted-Least-Squares Gradient Reconstruction," arXiv:1702.04518 [physics.flu-dyn], 2017.

[4]Zhang, F., *Research on Spatial Discretization Schemes for Finite Volume Method on Unstructured Grids*, Ph.D. thesis, Dalian University of Technology, 2017.

[5]Masatsuka, K., "I do like CFD, VOL.1, Second Edition," `http://www.cfdbooks.com`, 2013.

[6]Roe, P. L., "Approximate Riemann Solvers, Parameter Vectors, and Difference Schemes," *J. Comput. Phys.*, Vol. 43, 1981, pp. 357–372.

[7]Harten, A., Lax, P. D., and van Leer, B., "On Upstream Differencing and Godunov-Type Schemes for Hyperbolic Conservation Laws," *SIAM Rev.*, Vol. 25, No. 1, 1983, pp. 35–61.

[8]Nishikawa, H., "Beyond Interface Gradient: A General Principle for Constructing Diffusion Schemes," *Proc. of 40th AIAA Fluid Dynamics Conference and Exhibit*, AIAA Paper 2010-5093, Chicago, 2010.

[9]Nishikawa, H., "Two Ways to Extend Diffusion Schemes to Navier-Stokes Schemes: Gradient Formula or Upwinding," *20th AIAA Computational Fluid Dynamics Conference*, AIAA Paper 2011-3044, Honolulu, Hawaii, 2011.

[10]Nishikawa, H., "Robust and Accurate Viscous Discretization via Upwind Scheme - I: Basic Principle," *Comput. Fluids*, Vol. 49, No. 1, October 2011, pp. 62–86.

[11]Nishikawa, H., Nakashima, Y., and Watanabe, N., "Effects of High-Frequency Damping on Iterative Convergence of Implicit Viscous Solver," *J. Comput. Phys.*, Vol. 348, 2017, pp. 66–81.

[12]White, J., Nishikawa, H., and Baurle, R., "A 3-D Nodal-Averaged Gradient Approach for Unstructured-grid Cell-centered Finite-volume Methods for Application to Turbulent Hypersonic Flow," *SciTech 2020 Forum*, Orlando, FL, 2020, to be published as AIAA paper.

[13]Venkatakrishnan, V., "Convergence to Steady State Solutions of the Euler Equations on Unstructured Grids with Limiters," *J. Comput. Phys.*, Vol. 118, 1995, pp. 120–130.

[14]Seok Park, J., Hwan Yoon, S., and Kim, C., "Multi-Dimensional Limiting Process for Hyperbolic Conservation Laws on Unstructured Grids," *J. Comput. Phys.*, Vol. 229, 2010, pp. 788–812.

[15]Désidéri, J.-A. and Hemker, P. W., "Convergence Analysis of the Defect-Correction Iteration for Hyperbolic Problems," *SIAM J. Sci. Comput.*, Vol. 16, No. 1, 1994, pp. 88–118.

[16]Haider, F., Croisille, J.-P., and Courbet, B., "Stability Analysis of the Cell Centered Finite-Volume MUSCL Method on Unstructured Grids," *Numer. Math.*, Vol. 113, No. 4, 2009, pp. 555–600.

[17]Rusanov, V. V., "Calculation of Interaction of Non-Steady Shock Waves with Obstacles," *J. Compt. Math. Phys. USSR*, Vol. 1, 1961, pp. 267–279.
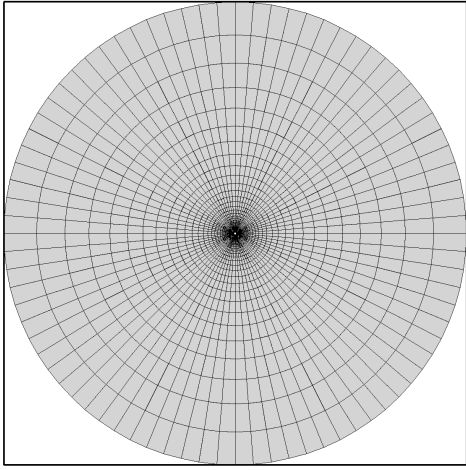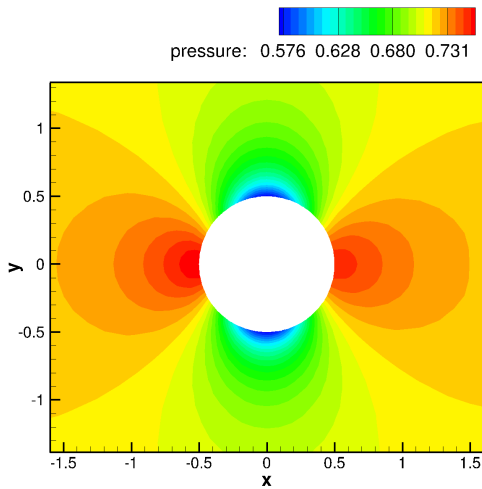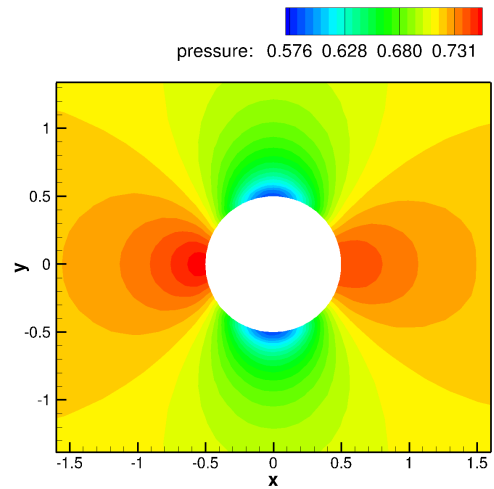
(a) Grid.
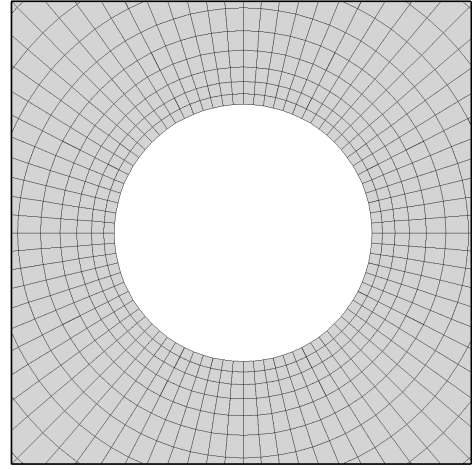
(b) Zoomed-in view.
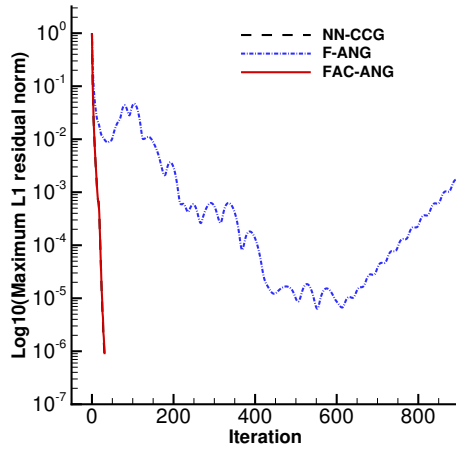
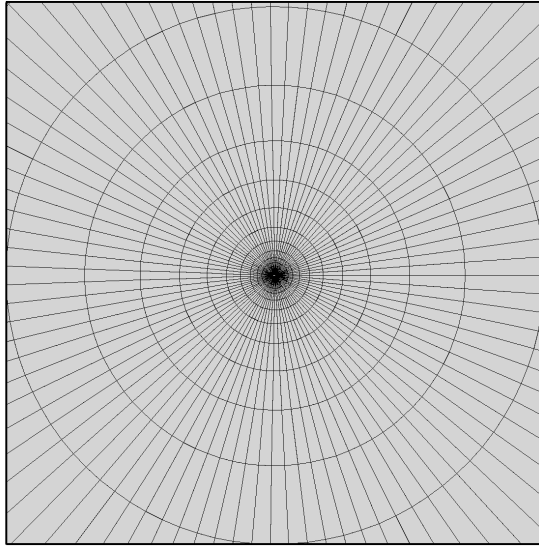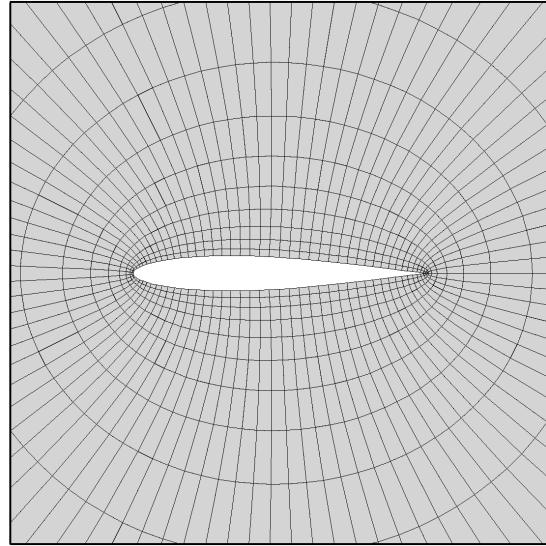

(c) Maximum residual versus iteration.
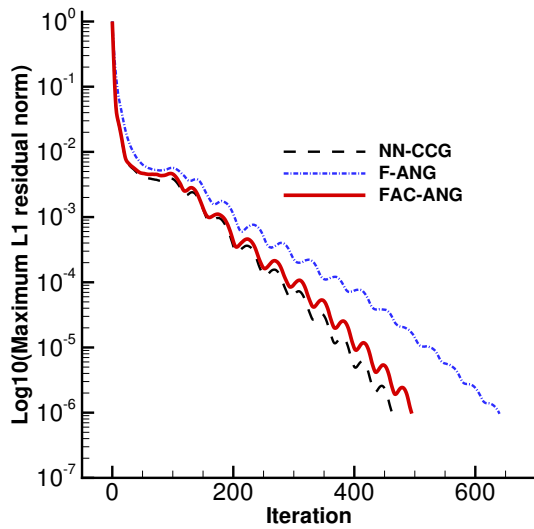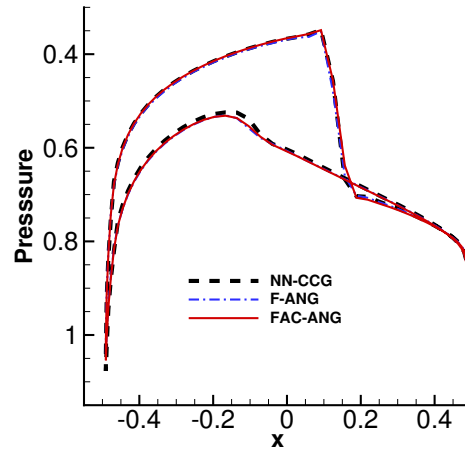


(d) NN-CCG.

(e) FAC-ANG.

Figure 2: Inviscid flow over a cylinder at $M_\infty = 0.3$ on a quadrilateral grid.
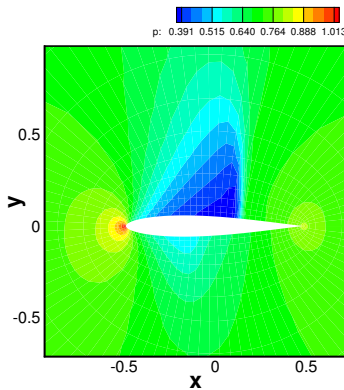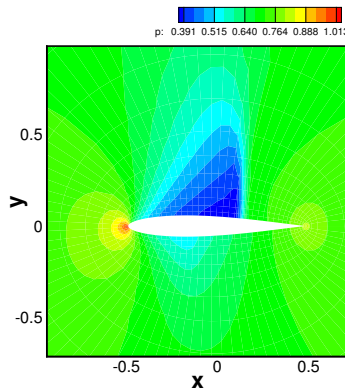
(a) Grid.

(b) Zoomed-in view.
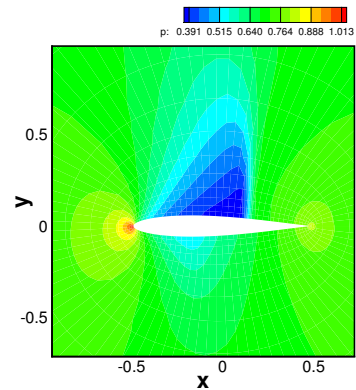
(c) Maximum residual versus iteration.

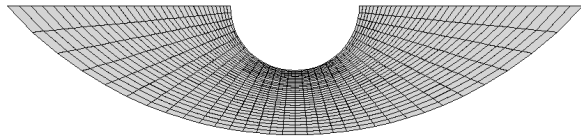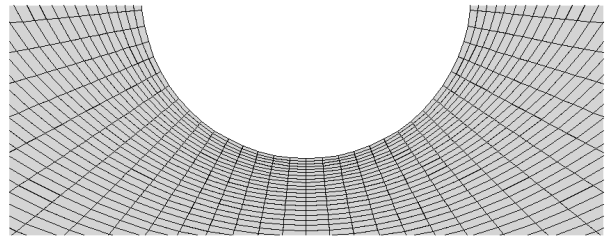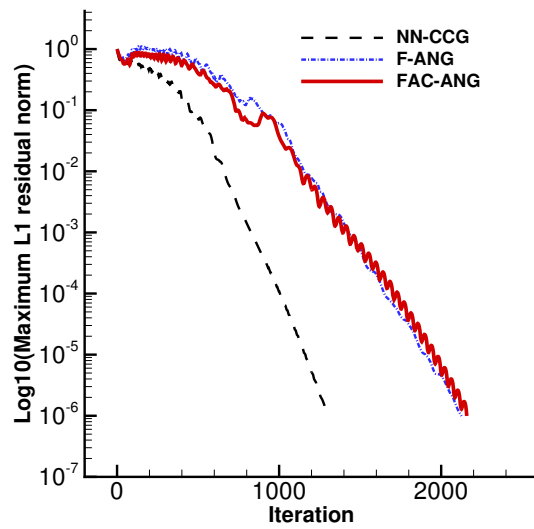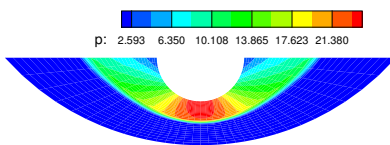(d) Pressure distribution.

(e) NN-CCG

(f) F-ANG

(g) FAC-ANG

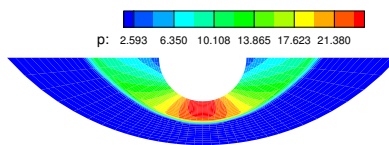Figure 3: Inviscid flow over a Joukowsky airfoil at $M_\infty = 0.85$ on a quadrilateral grid.
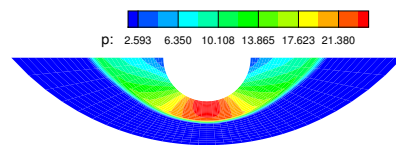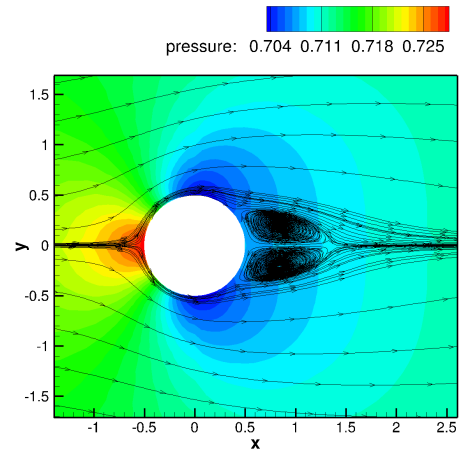
(a) Grid.



(b) Zoomed-in view.



(c) Maximum residual versus iteration.



(d) Pressure: NN-CCG.



(e) Pressure: F-ANG.



(f) Pressure: FAC-ANG.

Figure 4: Hypersonic flow over a cylinder at $M_\infty = 5.2$ on a quadrilateral grid.
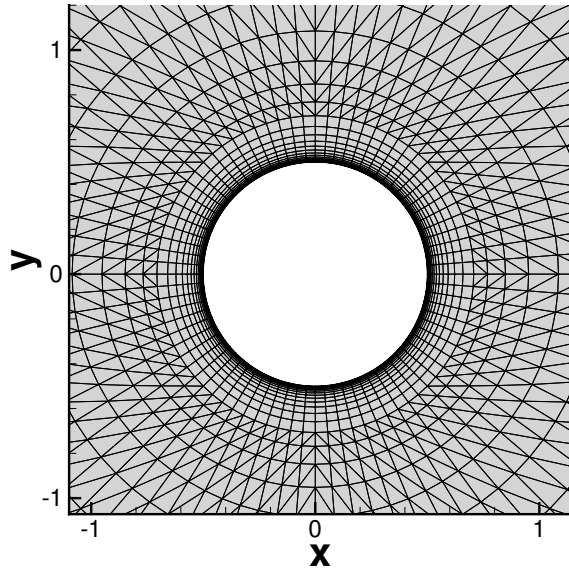
(a) Grid.
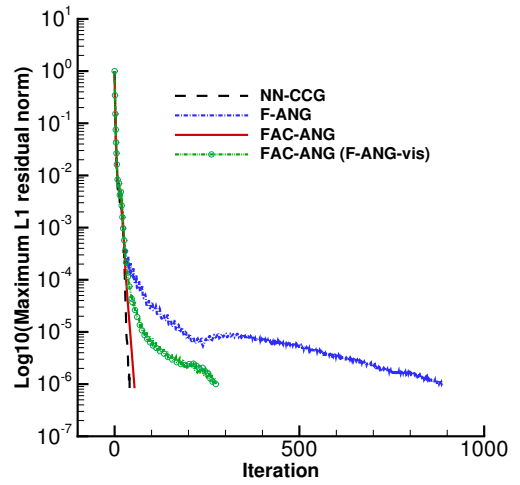


(b) Maximum residual versus iteration.
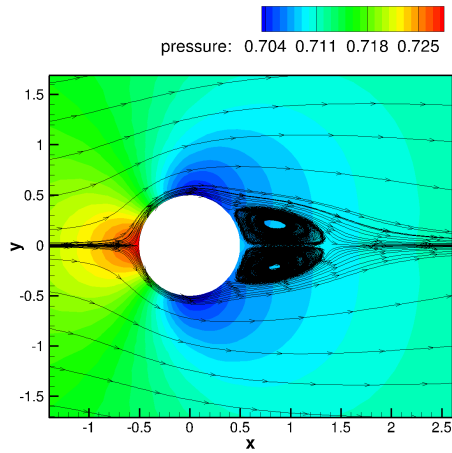


(c) NN-CCG.



(d) FAC-ANG.

Figure 5: Viscous flow over a cylinder at $M_\infty = 0.3$ and $Re_\infty = 40$ on a mixed grid.
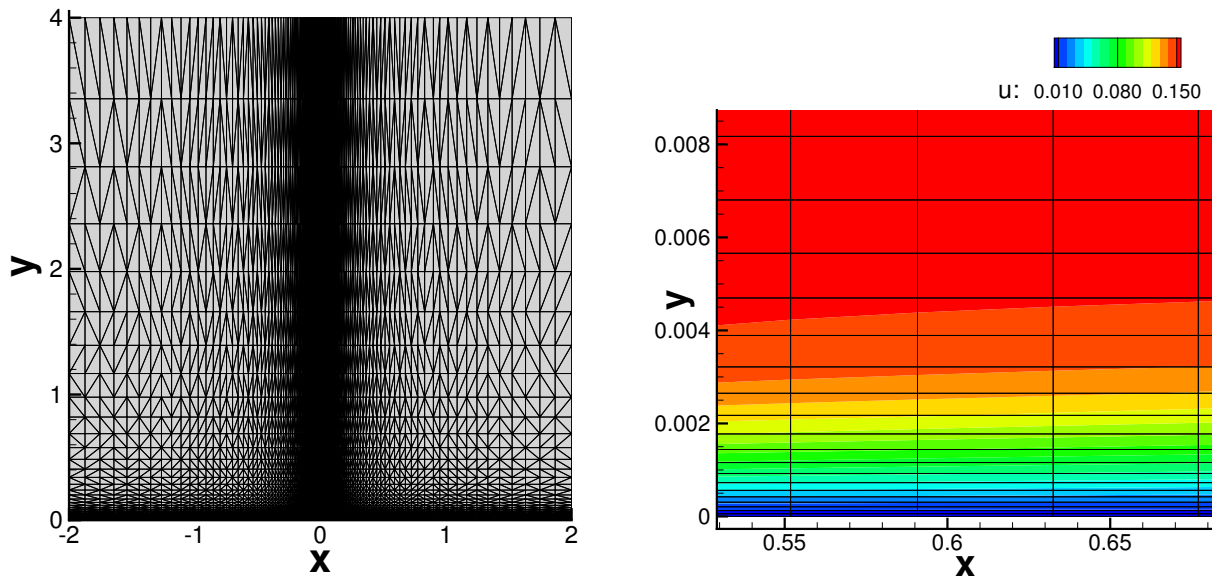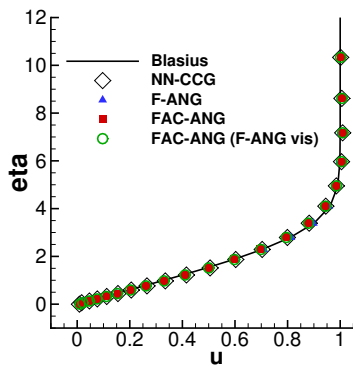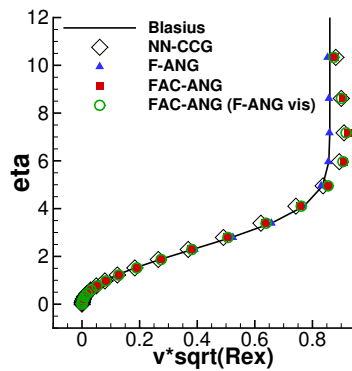
(a) Mixed grid.

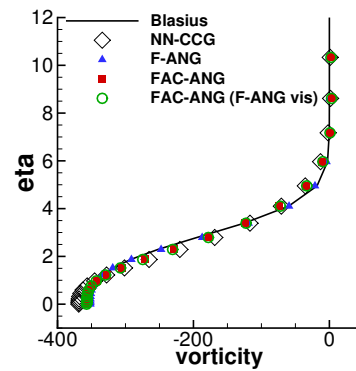(b) Zoomed-in view with a numerical solution.
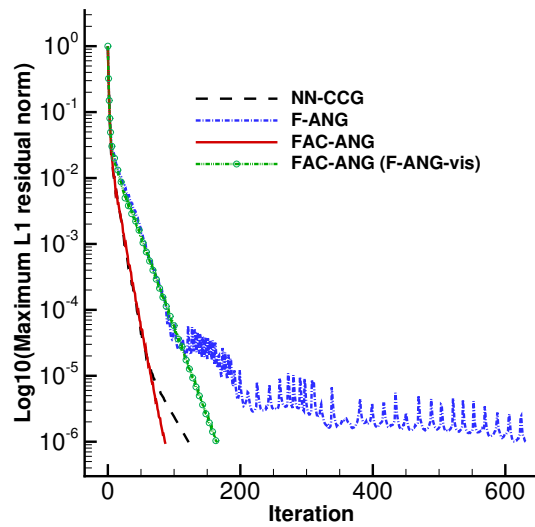


(c) Maximum residual versus iteration.



(d) Velocity $u$ at $x = 0.9$.

(e) Velocity $v$ at $x = 0.9$.

(f) Vorticity at $x = 0.9$.

Figure 6: Viscous flow over a flat plate on a mixed grid at $M_\infty = 0.15$ and $Re_\infty = 10^6$.